New Journal of Physics
The open access journal at the forefront of physics

Deutsche Physikalische Gesellschaft DPG IOP Institute of Physics

PAPER • OPEN ACCESS

Expanding the Lorentz concept in magnetism

To cite this article: G J Bowden *et al* 2019 *New J. Phys.* **21** 073063

New Journal of Physics
The open access journal at the forefront of physics

Deutsche Physikalische Gesellschaft DPG
IOP Institute of Physics

Published in partnership with: Deutsche Physikalische Gesellschaft and the Institute of Physics

PAPER

Expanding the Lorentz concept in magnetism

G J Bowden[1], G van der Laan[2], T Hesjedal[3] and R J Hicken[4]

[1] School of Physics and Astronomy, University of Southampton, SO17 1BJ, United Kingdom
[2] Magnetic Spectroscopy Group, Diamond Light Source, Didcot, OX11 0DE, United Kingdom
[3] Clarendon Laboratory, Oxford University, OX1 3PU, United Kingdom
[4] School of Physics and Astronomy, University of Exeter, Stocker Road, Exeter, Devon EX4 4QL, United Kingdom

E-mail: thorsten.hesjedal@physics.ox.ac.uk

Keywords: magnetic monolayers, Lorentz magnetic field, internal dipolar fields, ferromagnetic resonance, magnetic modeling

OPEN ACCESS

RECEIVED
17 May 2019

REVISED
26 June 2019

ACCEPTED FOR PUBLICATION
4 July 2019

PUBLISHED
30 July 2019

Abstract

In 1878, the Dutch physicist Hendrik Antoon Lorentz first addressed the calculation of the local electric field at an atomic site in a ferroelectric material, generated by all the other electric dipoles within the sample. This calculation, which applies equally well to ferromagnets, is taught in Universities around the World. Here we demonstrate that the Lorentz concept can be used to speed up calculations of the local dipolar field in square, circular, and elliptical shaped monolayers and thin films, not only at the center of the film, but across the sample. Calculations show that long elliptical and rectangular films should exhibit the narrowest ferromagnetic resonance (FMR) linewidth. In addition, discrete dipole calculations show that the Lorentz cavity field ($\mu_0 M/3$) does not hold in tetragonal films. Depending on the ratio (b/a), the local field can be either less/greater than ($\mu_0 M/3$): an observation that has implications for FMR. 3D simple cubic (SC) systems are also examined. For example, while most texts discuss the Lorentz cavity field in terms of a Lorentz sphere, the Lorentz cavity field still holds when a Lorentz sphere is replaced by a the Lorentz cube, but only in cubic SC, FCC and BCC systems. Finally, while the primary emphasis is on the discrete dipole–dipole interaction, contact is made with the continuum model. For example, in the continuous SC dipole model, just one monolayer is required to generate the Lorentz cavity field. This is in marked contrast to the discrete dipole model, where a minimum of five adjacent monolayers is required.

1. Introduction

In recent years there has been growing interest into incorporating thin magnetic films (100 μm–100 nm) into metamolecules [1–4] and magnonic devices [5, 6]. The properties of thin patterned magnetic films are therefore of importance. In general, such devices rely on exciting ferromagnetic resonance (FMR), which is dependent on the *local* dipolar field $\boldsymbol{B}_{\rm loc}(\boldsymbol{r})$ generated at site $\boldsymbol{r}$ by all the other dipoles within the sample (not the macroscopic field $\boldsymbol{B} = \mu_o(\boldsymbol{H} + \boldsymbol{M})$, see the discussion by Kittel [7, 8]). Here, we first review the calculation of the local field, as laid down by Lorentz [9][5] and Brown [10]. Secondly, we adapt the Lorentz method to monolayers and thin films. Thirdly, an extension of the Lorentz method is used to speed up calculation of local dipolar fields, as a function of position within a given thin film. Fourthly, we compare local dipolar fields in square, rectangular, circular, and elliptical shapes, paying particular attention to the local dipolar fields at the edges. In essence, the work presented here can be seen as an attempt to identify that shape of film (pattern) which should yield the narrowest FMR linewidth. Such experiments should have relevance in magnetic hybrid split ring resonator (SRR) metamolecules, where strong photon–magnon coupling occurs [2–4]. In the latter experiments, the permalloy and other magnetic films were simply patterned into small circular disks of ~100 μm diameter, primarily to suppress eddy currents. Little regard was paid as to how to strengthen the FMR/SRR (magnon/photon) interaction. In this paper, it is argued that the use of long rectangular or elliptical shapes should lead to

[5] Note. According to Kittel [8] the field due to polarization charges on the inside of a fictitious sphere was fist calculated by Lorentz in 1878.

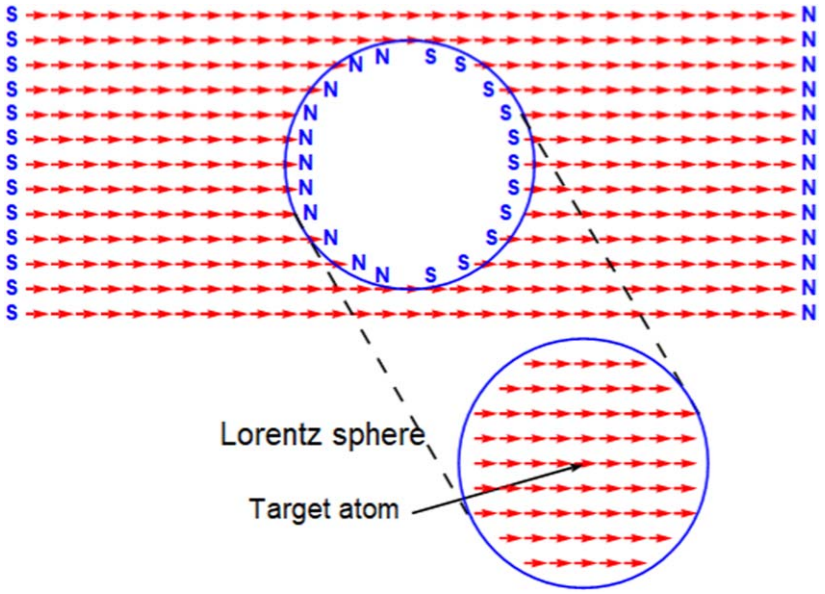

Figure 1. 2D schematic diagram showing a Lorentz sphere in a thick film. In reality, the 2D disk (2D rectangle) should be a 3D sphere (3D slab), respectively.

sharper FMR resonances, and hence stronger photon–magnon coupling. However, while the above provides some motivation for the present work, the results presented here, advance the Lorentz concept in basic magnetism, particularly in monolayers and thin films.

2. Brief review of magnetostatics

Using a uniformly magnetized ferromagnetic slab as an example, the local dipolar field at a target site $\boldsymbol{r}_i$ can be expressed in the form:

$$\boldsymbol{B}_{\rm loc}(\boldsymbol{r}_i) = \boldsymbol{B}_{\rm dip}(\boldsymbol{r}_i) + \boldsymbol{B}_{\rm Lor} + \boldsymbol{B}_{\rm demag} + \boldsymbol{B}_{\rm app}. \tag{1}$$

A schematic diagram, illustrating the origin of the $\boldsymbol{B}_{\rm dip}(\boldsymbol{r}_i)$, $\boldsymbol{B}_{\rm Lor}$, and $\boldsymbol{B}_{\rm demag}$ terms, can be seen in figure 1. Here:

$$\boldsymbol{B}_{\rm dip}(\boldsymbol{r}_i) = \frac{\mu_0}{4\pi}\sum_{j\neq i}^{\substack{\rm Lorentz\\ \rm Sphere}}\left(-\frac{\boldsymbol{\mu}_j}{r_{ij}^3} + 3\frac{(\boldsymbol{\mu}_j\cdot\boldsymbol{r}_{ij})\boldsymbol{r}_{ij}}{r_{ij}^5}\right);\ \boldsymbol{B}_{\rm Lor} = \frac{\mu_0\boldsymbol{M}}{3};\ \boldsymbol{B}_{\rm demag} = -\boldsymbol{D}.\boldsymbol{M}, \tag{2}$$

where the remaining symbols take on their usual meanings. So in addition to the applied field $\boldsymbol{B}_{\rm app}$, the actual local dipolar field $\boldsymbol{B}_{\rm loc}(\boldsymbol{r}_i)$ at the target atom consists of three terms. One, a contribution generated by all the dipoles within the Lorentz sphere: $\boldsymbol{B}_{\rm dip}(\boldsymbol{r}_i)$. Two, the Lorentz field $\boldsymbol{B}_{\rm Lor}$ generated by the free poles at the edges of the spherical hole (often referred to as the Lorentz cavity or remagnetizing field $\mu_0 M/3$). Three, a demagnetization field $\boldsymbol{B}_{\rm demag}$, generated by uncompensated magnetic poles at the extreme left and right of the slab. The contribution from all other dipoles, the vast majority, amounts to zero by a fundamental theorem of electrostatics (see appendix A). This theorem rests on two pillars. One, the magnetization in the sample with the Lorentz sphere removed, can be considered as *continuous*, as viewed from the center of the Lorentz sphere. Two, the divergence of the magnetization $\mathrm{div}\boldsymbol{M} = 0$, i.e. uniform magnetization regardless of shape.

In the following sections, we apply the Lorentz method to thin films and monolayers, where the concept of a Lorentz sphere is now meaningless.

3. Monolayer magnetostatics

For thin films, the dipole–dipole contribution to the local field $\boldsymbol{B}_{\rm loc}(\boldsymbol{r})$ at a given site can be determined by summing over all the fields generated by dipoles, within individual monolayers, and subsequently adding all the monolayer contributions together. This method works in thin films because, in general, only five monolayers are required [11].

Specifically, if all the magnetic moments within a given monolayer are parallel, the local field at the origin (0, 0, 0) in a simple cubic (SC) compound can be written in compact matrix form:

$$B_{\rm loc}(r) = \frac{\mu_0}{4\pi}\frac{1}{a^3}\sum_{\Delta k}\mu_k\begin{pmatrix} D_{xx}^{\Delta k} & 0 & 0 \\ 0 & D_{xx}^{\Delta k} & 0 \\ 0 & 0 & -2D_{xx}^{\Delta k}\end{pmatrix}\begin{pmatrix}\mu_x/\mu_k \\ \mu_y/\mu_k \\ \mu_z/\mu_k\end{pmatrix}. \tag{3}$$

Here (i) $\Delta k = 0$ refers to that monolayer which contains the target atom $\boldsymbol{r} = (0, 0, 0)$, while $\Delta k = \pm 1, \pm 2$ refers to the monolayers above and below the target monolayer, etc, (ii) the dimensionless term $\mathcal{D}_{xx}^{\Delta k}$ is a shorthand notation for the planewise summations

$$\mathcal{D}_{xx}^{\Delta k} = \sum_{\{i,j\}} D_{xx}^{ij\Delta k} \tag{4}$$

(iii)

$$D_{xx}^{ij\Delta k} = \frac{(3i^2 - r^2)}{r^5};\ r = \sqrt{i^2 + j^2 + \Delta k^2}. \tag{5}$$

(iv) The $\{i, j\}$ refer specifically to the positions of the moments $\{x, y\}$ within a given plane k, (v) $\Delta k = (k - k')$, (vi) the z-axis is normal to the film, in the direction of Δk, (vii) because of cubic symmetry $\mathcal{D}_{yy}^{\Delta k} = \mathcal{D}_{xx}^{\Delta k}$ *and* $\mathcal{D}_{xy}^{\Delta k} = \mathcal{D}_{xz}^{\Delta k} = \mathcal{D}_{yz}^{\Delta k} = 0$, (viii) the matrix is traceless, and (ix) all other symbols possess their usual meanings. Also, note that (i) this method only works, if all the magnetic moments μ_k within a given monolayer are parallel to each other, and (ii) in the Lorentz limit, the dipolar sums $\mathcal{D}_{xx}^{\Delta k}$ will give rise to the local field $\boldsymbol{B}_{\rm loc}(\boldsymbol{r})$, as described by equations (1)–(2).

In [11], it was shown that for a SC square monolayer film with $(2m + 1) \times (2m + 1)$ spins (m integer), the $\mathcal{D}_{xx}^{\Delta k}(m)$ converge asymptotically according to:

$$\mathcal{D}_{xx}^{\Delta k}(m) = \alpha_{\Delta k} - \frac{2\sqrt{2}}{m}. \tag{6}$$

In practice, the constants $\alpha_{\Delta k}$ are essentially zero for $|\Delta k| > 2$. Thus for a SC ferromagnetic thin film, only three numbers are required:

$$\alpha_0 = 4.516\,811;\ \alpha_{\pm 1} = -0.163\,7329;\ \alpha_{\pm 2} = -0.000\,278\,402. \tag{7}$$

So for an infinite film, $(m \to \infty)$:

$$\mathcal{D}_{xx}^{\Delta k}(m = \infty) = 4.516\,811 - 2 \times 0.163\,7329 - 2 \times 0.000\,2784 \cong \frac{4\pi}{3}. \tag{8}$$

Consequently, for an in-plane x-axis magnetization:

$$\boldsymbol{B}_{\rm loc}(\boldsymbol{r}) = \frac{\mu_0}{4\pi}\frac{\mu}{a^3}\frac{4\pi}{3}\boldsymbol{i} = \frac{\mu_0 M}{3}\boldsymbol{i}\ (=\boldsymbol{B}_{\rm Lor}). \tag{9}$$

This is exactly the same cavity or remagnetizing Lorentz field as that found at the center of the Lorentz sphere (see figure 1).

Finally, before leaving this section, we state that in the main we shall concentrate primarily on the properties of the dimensionless dipolar terms $\mathcal{D}_{xx}^{\Delta k}(m)$. In practice, such terms can be rapidly converted into dipolar fields using equations such as equation (9). However, this involves additional prefactors that reduce clarity of presentation. In addition, we shall also concentrate primarily on the properties of $\mathcal{D}_{xx}^{\Delta k}(m)$ with $\Delta k = 0$, since it is this monolayer which contributes the largest contribution to the local dipolar field.

4. The Lorentz method in monolayers

In [11] it was shown that the slowly converging term $2\sqrt{2}/m$ in equation (6) originates from demagnetizing fields at the edges of the film. This result allows us to adapt the Lorentz method to a square monolayer of spins, as illustrated schematically in figure 2.

Here, the Lorentz square, defined by $(2m_{\rm Lor} + 1) \times (2m_{\rm Lor} + 1)$ spins, is located in the center of the square film ($m > m_{\rm Lor}$). Thus for the target atom at the center of the film:

$$\mathcal{D}_{xx}^{\Delta k}(m) = \mathcal{D}_{xx}^{\Delta k}(m_{\rm Lor}) + \frac{2\sqrt{2}}{m_{\rm Lor}} - \frac{2\sqrt{2}}{m}. \tag{10}$$

The first term $\mathcal{D}_{xx}^{\Delta k}(m_{\rm Lor})$ is the discrete contribution from all the dipoles within the Lorentz square, the second term $2\sqrt{2}/m_{\rm Lor}$ is the monolayer equivalent of the remagnetizing Lorentz field, while the third term is the layer-equivalent demagnetizing contribution, arising from the free poles on the edges of the $m \times m$ square film. All contributions from other dipoles (the vast majority) amount to zero, as in the Lorentz method (see appendix A). Equivalently, in terms of magnetic field, for a uniformly magnetized monolayer, magnetized along the x-axis:

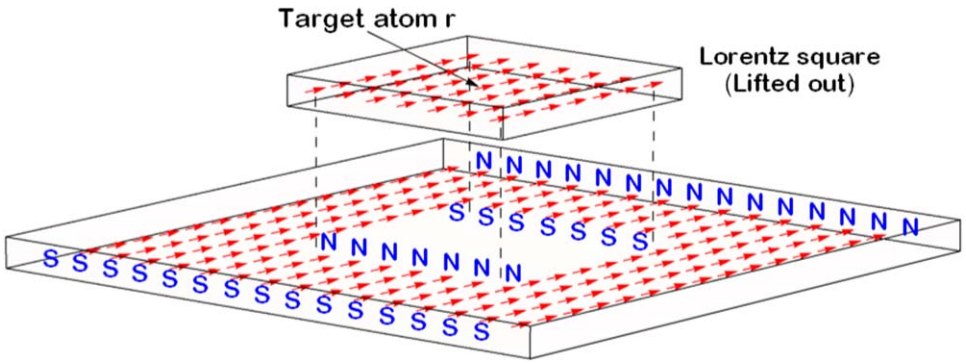

Figure 2. Schematic representation of the Lorentz method for a square monolayer of spins, showing the uncompensated North and South poles.

Table 1. (a) The Lorentz method applied to a SC monolayer using Lorentz squares of differing sizes: $\mathcal{D}^{0}_{xx}$ as a function of $m_{\rm Lor}$. (b) The Lorentz method applied to a SC monolayer using Lorentz squares of differing sizes: $\mathcal{D}^{\pm 1}_{xx}$ as a function of $m_{\rm Lor}$.

$m_{\rm Lor}$	$\mathcal{D}^{\pm 0}_{xx}(m_{\rm Lor})$	$2\sqrt{2}\,/\,m_{\rm Lor}$	$\mathcal{D}^{0}_{xx}(m_{\rm Lor}) + 2\sqrt{2}\,/\,m_{\rm Lor}$
20	4.378 87	0.141 421	4.520 29
50	4.460 80	0.056 5685	4.517 37
100	4.488 67	0.028 2843	4.516 95
250	4.505 52	0.011 3137	4.516 83
500	4.511 16	0.005 657	4.516 82
1000	4.513 98	0.002 828	4.516 808
2000	4.515 40	0.001 414 21	4.516 811
3000	4.515 87	0.000 943	4.516 811
(b)			
20	−0.301 261	0.141 421	−0.159 840
50	−0.219 711	0.056 5685	−0.163 142
100	−0.191 872	0.028 2843	−0.163 588
250	−0.175 023	0.011 3137	−0.163 709
500	−0.169 383	0.005 657	−0.163 726
1000	−0.166 559	0.002 828	−0.163 731
2000	−0.165 146	0.001 414 21	−0.163 732
3000	−0.164 675	0.000 943	−0.163 732

$$\boldsymbol{B}_{\rm loc}(\boldsymbol{r}) = \frac{\mu_0}{4\pi} M \sum_{\Delta k} \left(\mathcal{D}^{\Delta k}_{xx}(m_{\rm Lor}) + \frac{2\sqrt{2}}{m_{\rm Lor}} - \frac{2\sqrt{2}}{m} \right) \boldsymbol{i}, \left(M = \frac{\mu}{a^3} \right). \tag{11}$$

However, there is one big difference between the original Lorentz method and that of the monolayer method presented here. In the original Lorentz model, the sum over all the dipoles enclosed by the Lorentz sphere is zero: $\boldsymbol{B}_{\rm dip}(\boldsymbol{r}_i) \equiv 0$ for a SC lattice. However, this is not the case for the sum over the spins in a SC Lorentz square. Indeed, this term is the major contributor to the value of $\mathcal{D}^{\Delta k}_{xx}(m \to \infty)$: a point illustrated in tables 1(a), (b) for $\mathcal{D}^{0}_{xx}$, $\mathcal{D}^{\pm 1}_{xx}$, respectively.

Next, we observe that the Lorentz method allows for a fast determination of $\mathcal{D}^{\Delta k}_{xx}(m \to \infty)$. From equation (10), for $m \to \infty$, $\mathcal{D}^{\Delta k}_{xx}(m \to \infty) \to \mathcal{D}^{\Delta k}_{xx}(m_{\rm Lor}) + (2\sqrt{2})\,/\,m_{\rm Lor}$. Thus we should be able to determine the value of $\mathcal{D}^{\Delta k}_{xx}(m \to \infty)$, using relatively small values of $m_{\rm Lor}$. This trick is illustrated in tables 1(a), (b). For example, if this method is to work the last column in say table 1(a), should read 4.516 81. For $m_{\rm Lor} \geqslant 1000$, the error is negligible. However, even for $m_{\rm Lor}$ as small as 50, the deviation from the saturation value is only +1.2%. Similar conclusions also hold for $\mathcal{D}^{\pm 1}_{xx}$ (see table 1(b)).

In conclusion, it is clear that the Lorentz method can be used to examine and speed up the determination of the local dipolar fields in a given monolayer, using relatively small values of the Lorentz square $(2m_{\rm Lor} + 1) \times (2m_{\rm Lor} + 1)$. It is also clear that such tables can be used to answer the question: 'what is the value of $m_{\rm Lor}$ required for a given accuracy?' However, rather surprisingly, we find that quite small values $m_{\rm Lor} \approx 50$ are sufficient.

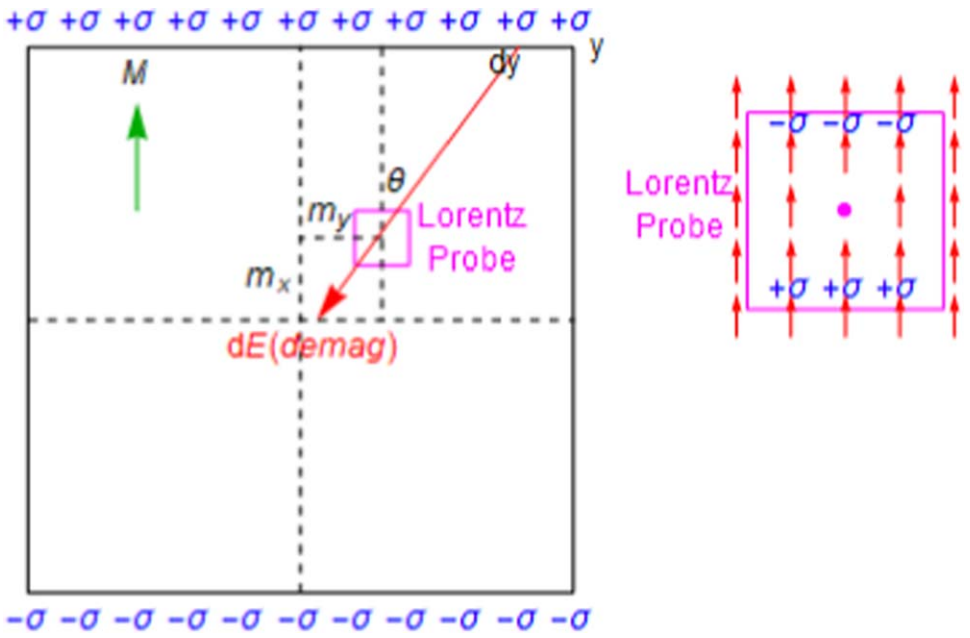

Figure 3. Schematic diagram showing the Lorentz probe (magenta) inside a monolayer square film. The integers m_x and m_y determine the direction of travel. The actual size of the Lorentz probe on the right is grossly under-exaggerated.

Indeed, this observation allows us to examine the variation of the local dipolar field across a given monolayer or thin film, as discussed in the next section.

5. Local dipolar field spatial variation in a uniformly magnetized square thin film

So far, we have concentrated on calculating the local dipolar field at the center of say a sphere or thin film. Here, we show that the Lorentz method can be used to speed up the calculation of the local dipolar-field variations across a uniformly magnetized thin film.

Instead of fixing the position of the Lorentz square in the center of the film, we now allow the Lorentz square to travel (metaphorically) in both the x and y directions. This situation is illustrated schematically in figure 3. Here we can think of the Lorentz square as a Lorentz probe which we move around the film. Next, we use the surface charge analogy of demagnetization fields, to work out the value of the demagnetizing field at a given position within the film, arising from the free poles on the edges of the film. Note that a free north (south) pole, corresponds to a negative (positive) charge, respectively. Thus the demagnetizing field is in the same direction as the equivalent electric field.

If we set σ equal to the charge per unit length the charge dq at y in a small region dy is given by:

$$\mathrm{d}q = \sigma \mathrm{d}y. \tag{12}$$

This charge will give rise to an electric field d$\boldsymbol{E}$ at the target atom, located in the center of the Lorentz square (red)

$$\mathrm{d}E = \frac{\sigma \mathrm{d}y}{r^2}(-\hat{r}). \tag{13}$$

Next, we observe that:

$$\tan\theta = \frac{y - m_y a}{(m - m_x)a}. \tag{14}$$

Thus:

$$\mathrm{d}y = \frac{(m - m_x)a}{\cos^2\theta}\mathrm{d}\theta. \tag{15}$$

Also:

$$r\cos\theta = (m - m_x)a. \tag{16}$$

Consequently, on combining equations (12)–(16) we find:

$$\mathrm{d}E = -\frac{\sigma \mathrm{d}\theta}{(m - m_x)a}\hat{\boldsymbol{r}}. \tag{17}$$

Thus the total electric field, arising from the positive charges on the top of the film, is given by:

$$\begin{aligned} E_x^t &= -\frac{\sigma}{(m - m_x)a}\int_{-\theta_2}^{\theta_1} \cos\theta \mathrm{d}\theta = -\frac{\sigma[\sin\theta_1 + \sin\theta_2]}{(m - m_x)a} \\ E_y^t &= -\frac{\sigma}{(m - m_x)a}\int_{-\theta_2}^{\theta_1} \sin\theta \mathrm{d}\theta = +\frac{\sigma[\cos\theta_1 - \cos\theta_2]}{(m - m_x)a}. \end{aligned} \tag{18}$$

Here the angle θ is swept from θ_1 to $-\theta_2$, as indicated by the dotted red lines in figure 3, specifically:

$$\theta_1 = \tan^{-1}\left(\frac{m - m_y}{m - m_x}\right);\ \theta_2 = \tan^{-1}\left(\frac{m + m_y}{m - m_x}\right). \tag{19}$$

Likewise from the negative charges at the bottom of the film:

$$\begin{aligned} E_x^b &= -\frac{\sigma[\sin\theta_1' + \sin\theta_2']}{(m + m_x)a} \\ E_y^b &= \frac{\sigma[\cos\theta_2' - \cos\theta_1']}{(m + m_x)a}, \end{aligned} \tag{20}$$

where:

$$\theta_1' = \tan^{-1}\left(\frac{m - m_y}{m + m_x}\right);\ \theta_2' = \tan^{-1}\left(\frac{m + m_y}{m + m_x}\right). \tag{21}$$

So, for example, at the center of the square, $m_x = m_y = 0$, yielding $\theta_1 = \theta_2 = \theta_1' = \theta_2' = \pi/4$ Thus:

$$E_x^{\mathrm{tot}} = E_x^t + E_x^b = -\frac{2\sqrt{2}\sigma}{ma};\ E_y^{\mathrm{tot}} = 0 \tag{22}$$

in accord with [11].

Proceeding in this manner, we have calculated $\mathcal{D}_{xx}^0(m_x, m_y)$ as a function of position within a square film with m set equal to 5000, i.e. in excess of a 10^8 spins. To do this we have set the size of the Lorentz square (the probe) $m_{\mathrm{Lor}} = 50$. This small value does not yield the most accurate value of $\mathcal{D}_{xx}^0$ $(m \to \infty)$. However it does allow us to approach the edge of the film to within $\Delta m = -50$. The results are detailed in figure 4(a), where it will be observed that most of the film is characterized by a constant value, close to 4.516, except at the film edges where it falls sharply. We shall refer to these two sharp falls as the *cliff edges* at the North and South poles of the film.

Concomitantly, in addition to the changes in the magnitude of $\mathcal{D}_{xx}^0$, transverse fields (y-axis) are also generated by the demagnetization fields. Their amplitudes, which we shall denote by the cross term $\mathcal{D}_{xy}^0$, are summarized in figure 4(b). Note that the amplitude of the $\mathcal{D}_{xy}^0$ is close to zero for most of the film, except at the corners where it changes quite rapidly.

Finally, the local dipolar field, across the sample, can be determined using the matrix formulation:

$$\boldsymbol{B}_{\mathrm{loc}}(r) = \frac{\mu_0}{4\pi}\frac{\mu}{a^3}\sum_{\Delta k}\mu_k \begin{pmatrix} \mathcal{D}_{xx}^{\Delta k} & \mathcal{D}_{xy}^{\Delta k} & 0 \\ \mathcal{D}_{xy}^{\Delta k} & \mathcal{D}_{xx}^{\Delta k} & 0 \\ 0 & 0 & -2\mathcal{D}_{xx}^{\Delta k} \end{pmatrix} \begin{pmatrix} \mu_x/\mu_k \\ 0 \\ 0 \end{pmatrix}. \tag{23}$$

Here it is understood that (i) the $\mathcal{D}_{xx}^{\Delta k}$ etc are now position dependent, and (ii) the demagnetization fields are now all included in the $\mathcal{D}_{xy}^{\Delta k}$ etc terms. However it is also clear from an inspection of figures 4(a), (b) that the magnitude of the off-diagonal terms, at least for square films, is generally much smaller than their diagonal counterparts. Another notable features in figure 4(a) is the apparent constancy of $\mathcal{D}_{xx}^0$ (top and bottom) at the edges parallel to $\boldsymbol{M}$. Of course, it must be stressed that both diagrams (figures 4(a), (b)) only detail the magnitude of the $\mathcal{D}_{xx}^0$ and $\mathcal{D}_{xy}^0$ to within 50 atoms from the edges of the film. So while these figures detail the variation of the two terms across the vast majority of the 10^8 spins in the film, there is the possibility that both $\mathcal{D}_{xx}^0$ and $\mathcal{D}_{xy}^0$ may change even more dramatically as we approach the actual edges of the film. To investigate this situation, in more detail, we have examined the properties of a smaller film of 501×501 spins, this time going right up the edge of the film. The results can be seen in figures 5(a), (b).

From an examination of figure 5(a) it will be seen that the variation of $\mathcal{D}_{xx}^0$ parallel to the magnetization **M**, changes dramatically $(4.51 \to 1)$ at the North and South pole *cliff edges* of the film. However, perhaps surprisingly, $\mathcal{D}_{xx}^0$ perpendicular to the magnetization **M**, is relatively constant, only changing modestly right at

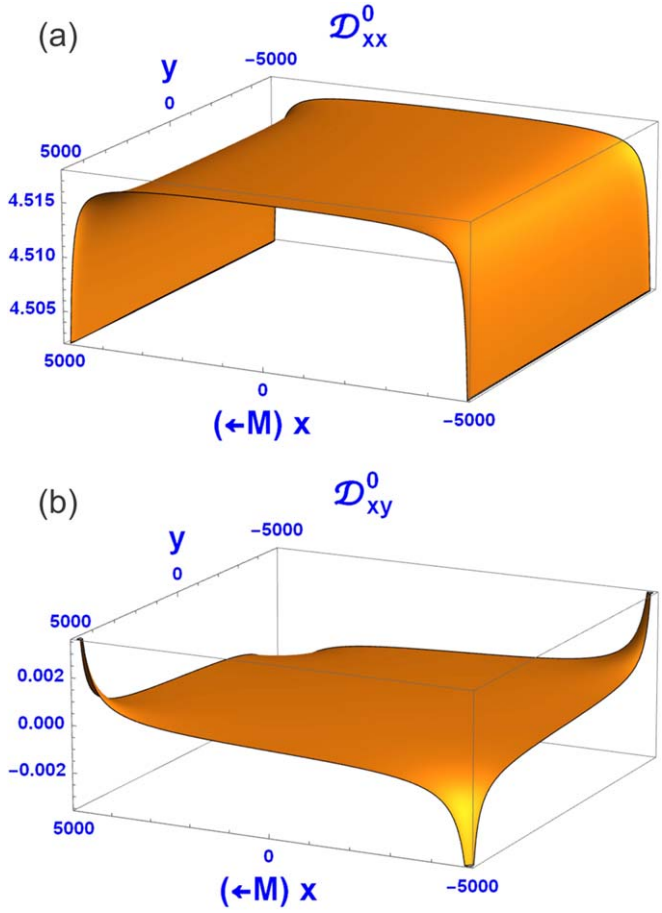

Figure 4. (a) Variation of $\mathcal{D}^0_{xx}$ as a function of position within a uniformly magnetized monolayer magnetized along the positive x-axis. (b) Variation of $\mathcal{D}^0_{xy}$ as a function of position within a uniformly magnetized monolayer magnetized along the positive x-axis. This will give rise to small displacements of the spins away from the x-axis magnetization in the $\pm y$ directions.

the very edge of the film (4.51 $\rightarrow$ 4.66). These observations therefore, suggest that if we wish to maximize the number of spins with the same local dipolar field, it is best to choose elongated rectangular films with the long axis parallel to the magnetization **M**. In fact, it is possible to put this statement on a semi-quantitative footing, by calculating the mean value and variance of say $\mathcal{D}^0_{xx}$ across the sample. The results can be seen in figures 6(a), (b), for ever increasing rectangular shapes.

From the $k = 0$ FMR point of view, the actual situation is, of course, more complicated than that implied by mean values and standard deviations. In practice, both the North and South pole cliff edges, will almost certainly lead to *pinning* at these edges of the film (different FMR frequency). This situation is examined in more detail in appendix B, where it is argued that (i) if the spin wave mode $k = \pi/l$ is excited, where l is the length of the film in the direction of the magnetization, and (ii) the shift in resonance is say $1/10^{\text{th}}$ of the inhomogeneous linewidth, then Kittel's FMR equations are still, essentially, valid. Of course, both the North and South pole *cliff-edges* can be avoided entirely, if a long rectangular strip is turned into a flattened ring. However, such 3D geometries will limit applications.

In the next section, we examine the local dipolar field across elliptically shaped monolayer or thin films. In practice, there are significant differences between rectangular and elliptical thin films.

6. Local dipolar fields in a uniformly magnetized elliptical disk

First, we obtain an expression for the demagnetization factor for a target atom at the geometric center of a monolayer in the form of an elliptical disk.

The equation of an ellipse takes the form:

$$\left(\frac{x}{a}\right)^2 + \left(\frac{y}{b}\right)^2 = 1. \tag{24}$$

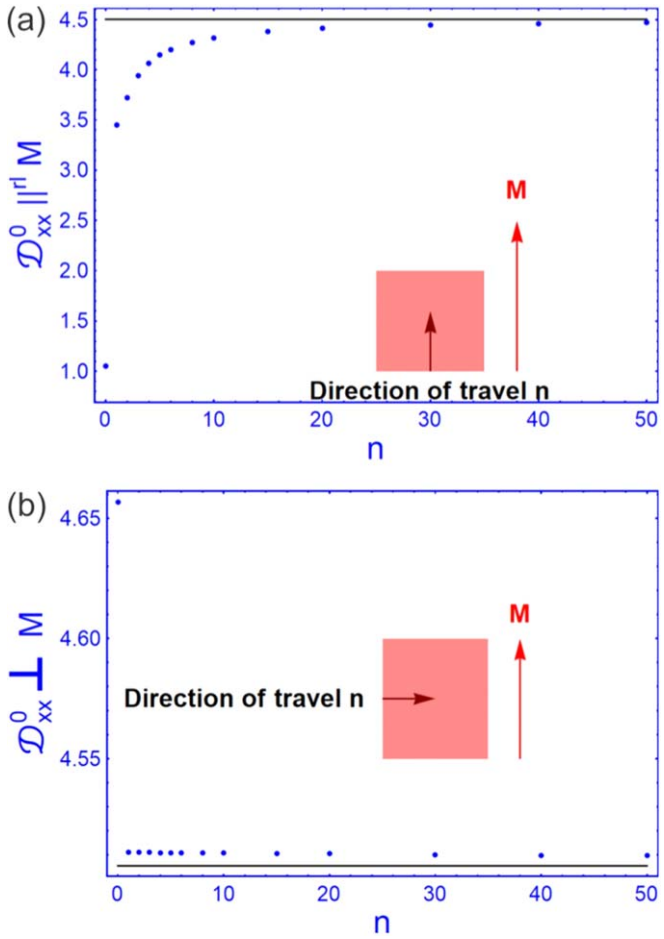

Figure 5. (a) $\mathcal{D}^0_{xx}$ parallel to the magnetization **M**, as a function of distance from the edge of the film. The dots signify the discrete value of $\mathcal{D}^0_{xx}$, in the direction of travel. The continuous line is the saturation value at the center of the film. (b) $\mathcal{D}^0_{xx}$ perpendicular to the magnetization **M**, as a function of distance from the edge of the film. The dots signify the value $\mathcal{D}^0_{xx}$, in the direction of travel. The continuous line is the saturation value at the center of the film.

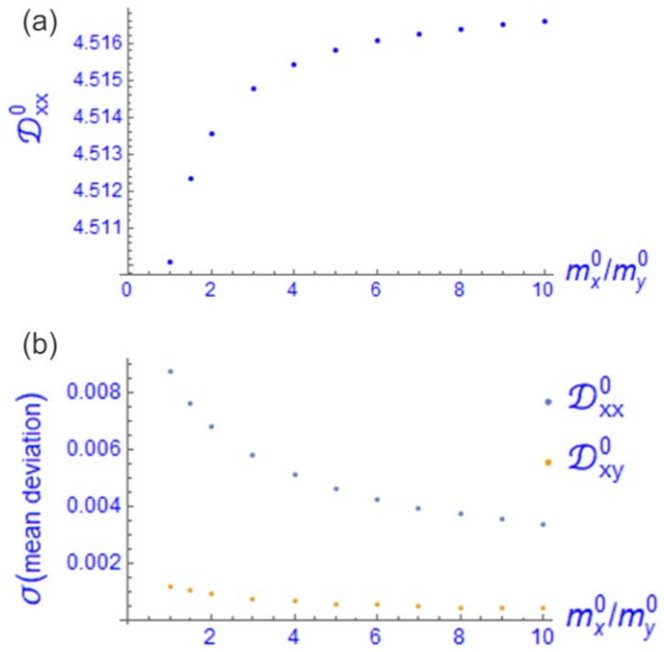

Figure 6. (a) Mean value of $\mathcal{D}^0_{xx}$ for rectangular films. The saturation value is $\mathcal{D}^0_{xx} = 4.516\,81$. (b) Standard deviation of $\mathcal{D}^0_{xx}$ and $\mathcal{D}^0_{xy}$ for rectangular films. The mean value for $\mathcal{D}^0_{xy}$ is always zero (see figure 4(b)).

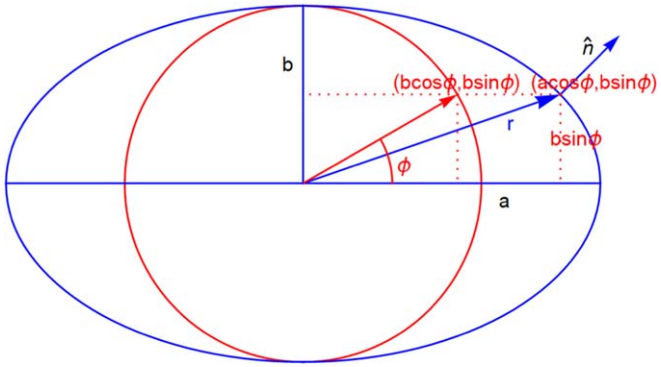

Figure 7. The parametric representation of an ellipse. The red circle is used as a construct for the blue ellipse.

Here, we observe the usual convention that the axes (a, b) are associated with the (long, short) axes, respectively, i.e. the ellipticity $\varepsilon = b/a \leqslant 1$. Unfortunately, this symbolism clashes with our earlier definition of a as the unit length of the SC lattice. So ultimately, it will be necessary to replace the elliptical length a by $m_a a$, where m_a is an integer.

In practice, it is convenient to use the parametric representation of an ellipse:

$$x = a\cos\phi,\ y = b\sin\phi, \tag{25}$$

where ϕ is measured from the long axis of the ellipse, and $a \geqq b$. The situation is illustrated in figure 7.

First, we need an expression for the charge distribution around the edges of the ellipse. In the parametric representation, the tangent to the ellipse at a general point (x, y) takes the form:

$$\boldsymbol{t} = \mathrm{d}x\,\boldsymbol{i} + \mathrm{d}y\,\boldsymbol{j} = -a\sin\phi\,\mathrm{d}\phi\,\boldsymbol{i} + b\cos\phi\,\mathrm{d}\phi\,\boldsymbol{j}. \tag{26}$$

So a normalized vector $\hat{\boldsymbol{n}}$, normal to the tangent $\boldsymbol{t}$, is given by:

$$\hat{\boldsymbol{n}} = \frac{\varepsilon\cos\phi\,\boldsymbol{i}}{\sqrt{\sin^2\phi + \varepsilon^2\cos^2\phi}} + \frac{\sin\phi\,\boldsymbol{j}}{\sqrt{\sin^2\phi + \varepsilon^2\cos^2\phi}}. \tag{27}$$

For the charge distribution as a function of ϕ, we are interested in the projection of the normal onto the direction of magnetization (the a (x)-axis). Thus the charge distribution scales as:

$$\sigma(\phi) = \frac{\sigma\,\varepsilon\cos\phi}{\sqrt{\sin^2\phi + \varepsilon^2\cos^2\phi}}. \tag{28}$$

Note that if $\varepsilon = 1$, $\sigma(\phi) \to \sigma\cos\phi$, i.e. that for a circle, as expected [11].

Next, from equation (25) we have:

$$r = a\sqrt{\cos^2\phi + \varepsilon^2\sin^2\phi}\,. \tag{29}$$

So a portion $\mathrm{d}s$ around the ellipse is given by:

$$\mathrm{d}s = a\sqrt{\sin^2\phi + \varepsilon^2\cos^2\phi}\,\mathrm{d}\phi. \tag{30}$$

Given that the charge on the ellipse scales as $\sigma_a(\phi)\mathrm{d}s$, we obtain:

$$\mathrm{d}E = \frac{\sigma(\phi)\mathrm{d}s}{r^2}\frac{-\hat{\boldsymbol{i}}\cos\phi - \hat{\boldsymbol{j}}\,\varepsilon\sin\phi}{\sqrt{\cos^2\phi + \varepsilon^2\sin^2\phi}}. \tag{31}$$

Thus:

$$E_a = -\frac{\sigma}{a}\left(\frac{\varepsilon\cos^2\phi}{(\cos^2\phi + \varepsilon^2\sin^2\phi)^{3/2}}\right)\mathrm{d}\phi. \tag{32}$$

On integrating therefore:

$$E_a = -\frac{\sigma}{a}\int_0^{2\pi}\left(\frac{\varepsilon\cos^2\phi}{(\cos^2\phi + \varepsilon^2\sin^2\phi)^{\frac{3}{2}}}\right)\mathrm{d}\phi,\ (0 \leqslant \varepsilon \leqslant 1). \tag{33}$$

In practice, analytic forms can be obtained for the above integrals, if the ellipticity ε can be expressed in the form of a fraction:

Table 2. The Lorentz method applied to a SC lattice using an elliptical monolayer with $\varepsilon = 1/2$, for various integer m_a along the a-axis. Note that the last column rapidly approaches 4.516 811, i.e. the value of $\mathcal{D}^0_{xx}(m_a \to \infty)$ (see [12, 14]). It will also be observed that even for m_a as small as 50, the error in $\mathcal{D}^0_{xx}(50) + \beta_a/50$ is very small, namely +1.1%.

m_a	$\mathcal{D}^0_{xx}(m_a)$	β_a/m_a	$\mathcal{D}^{\Delta k}_{xx}(m \to \infty) = \mathcal{D}^0_{xx}(m_a) + \beta_a/m_a$
50	4.4669	0.050 4245	4.517 32
100	4.491 73	0.025 2123	4.516 94
250	4.506 74	0.010 0849	4.516 82
500	4.511 77	0.005 042 45	4.516 81
1000	4.514 29	0.002 521 23	4.516 81
2000	4.515 55	0.001 260 61	4.516 81
3000	4.515 97	0.000 840 409	4.516 81

$$\varepsilon = \frac{p}{q}. \tag{34}$$

We find:

$$E_a = -\frac{\sigma\varepsilon}{a}\frac{4q^2}{q^2 - p^2}\left[\mathrm{K}\left(\frac{q^2 - p^2}{q^2}\right) - E\left(\frac{q^2 - p^2}{q^2}\right)\right](0 \leqslant \varepsilon \leqslant 1), \tag{35}$$

where K and E are elliptic integrals. Alternatively, in terms of α and β exponents, we have:

$$\mathcal{D}^{\Delta k}_{xx}(m_a) = \alpha^{\Delta k}_{xx} - \frac{\beta_a}{m_a}, \tag{36}$$

where the exponent β_a is given by:

$$\beta_a = -\frac{p}{q}\frac{4q^2}{q^2 - p^2}\left[K\left(\frac{q^2 - p^2}{q^2}\right) - E\left(\frac{q^2 - p^2}{q^2}\right)\right]. \tag{37}$$

Similarly, for magnetization along the shorter b-axis:

$$\mathcal{D}^{\Delta k}_{yy}(m_a) = \alpha^{\Delta k}_{yy} - \frac{\beta_b}{m_a}, \tag{38}$$

where β_b is given by:

$$\beta_b = -\frac{p}{q}\frac{4q^2}{q^2 - p^2}\left[K\left(\frac{q^2 - p^2}{q^2}\right) - \frac{q^2}{p^2}E\left(\frac{q^2 - p^2}{q^2}\right)\right]. \tag{39}$$

Note that if the eccentricity $\varepsilon = 1$, $\beta_a = \beta_b = \pi$, i.e. that for a circle. Also if $\varepsilon \to 0$, i.e. $a \gg b$, then $\beta_a \to 0$, which is to be expected. As the ellipse becomes more and more 'rod-like', the *charge* is now concentrated at the *ends* of the rod.

Next, some numerical calculations for an ellipse with $\varepsilon = 1/2$, are summarized in table 2. Once again, as with square monolayers, it is clear that the value of $\mathcal{D}^{\Delta k}_{xx}(m \to \infty)$ can be obtained using quite small elliptical disks. As with square monolayers discussed earlier, small elliptical Lorentz disks can be used to probe the variation of magnetic fields across larger elliptical monolayers.

Finally, before leaving this section we state that $\mathcal{D}^0_{xx}(m_a)$ and $\mathcal{D}^0_{yy}(m_a)$ terms can be fitted with the asymptotic formula:

$$\begin{aligned}\mathcal{D}^0_{xx}(m_\mathrm{a}) &= 4.516\,81 - 2.520\,75/m_a \\ \mathcal{D}^0_{yy}(m_a) &= 4.516\,81 - 7.168\,31/m_a.\end{aligned} \tag{40}$$

The first number $\alpha^{\Delta k}_{xx} = \alpha^{\Delta k}_{yy} = 4.516\,81$ is, of course, to be expected. The β_a (β_b) exponents can be calculated using equations (37) and (39). We find 2.521 23 (7.167 22), respectively, which compare favorably with the exponents of equation (40), obtained with a least squares fitting program.

In summary, we have obtained expressions for the local dipolar field at the center of an ellipse. In the following section, we use our extension of the Lorentz method to examine the local dipolar field at points other than that at the center of the ellipse.

7. The demagnetizing field at an arbitrary point in a ferromagnetic elliptical monolayer

First, it is necessary to obtain an expression for the demagnetizing field, at an arbitrary point within the disk, arising from free-poles on edges of a uniformly magnetized elliptical disk.

A general point $\boldsymbol{r}$ on the edge of the elliptical disk is given by:

$$\boldsymbol{r} = a(\cos\phi\ \hat{\boldsymbol{i}} + \varepsilon\ \sin\phi\ \hat{\boldsymbol{j}}). \tag{41}$$

Likewise, a point within the disk can be written:

$$\boldsymbol{r}_1 = a_1(\cos\phi_1\hat{\boldsymbol{i}} + \varepsilon\ \sin\phi_1\ \hat{\boldsymbol{j}}),\ (a_1 \leqslant a). \tag{42}$$

Thus the electric field at $\boldsymbol{r}_1$ due to the surface charge at $\boldsymbol{r}$ is given by:

$$\begin{aligned} \mathrm{d}\boldsymbol{E} &= \frac{\sigma(\phi)\mathrm{d}s}{|\boldsymbol{r}_1 - \boldsymbol{r}|^2}\frac{\boldsymbol{r}_1 - \boldsymbol{r}}{\sqrt{|\boldsymbol{r}_1 - \boldsymbol{r}|^2}} \\ &= \frac{\sigma\ \varepsilon\ \cos\phi}{\sqrt{\sin^2\phi + \varepsilon^2\cos^2\phi}}a\sqrt{\sin^2\phi + \varepsilon^2\cos^2\phi}\,\mathrm{d}\phi\frac{\boldsymbol{r}_1 - \boldsymbol{r}}{(|\boldsymbol{r}_1 - \boldsymbol{r}|^2)^{\frac{3}{2}}} \\ &= a\ \sigma\ \varepsilon\ \cos\phi\ \mathrm{d}\phi\frac{(a_1\cos\phi_1 - a\cos\phi)\hat{\boldsymbol{i}} + \varepsilon(a_1\sin\phi_1 - a\sin\phi)\hat{\boldsymbol{j}}}{[(a_1\cos\phi_1 - a\cos\phi)^2 + \varepsilon^2(a_1\sin\phi_1 - a\sin\phi)^2\,]^{3/2}}. \end{aligned} \tag{43}$$

Proceeding in this manner, we find:

$$\begin{aligned} E_x = E_a &= \int_0^{2\pi}\frac{(a\ \sigma\ \varepsilon\ \cos\phi)(a_1\cos\phi_1 - a\cos\phi)}{[(a_1\cos\phi_1 - a\cos\phi)^2 + \varepsilon^2(a_1\sin\phi_1 - a\sin\phi)^2\,]^{3/2}}\mathrm{d}\phi\hat{\boldsymbol{i}} \\ E_y = E_b &= \int_0^{2\pi}\frac{(a\ \sigma\ \varepsilon^2\ \cos\phi)(a_1\sin\phi_1 - a\sin\phi)}{[(a_1\cos\phi_1 - a\cos\phi)^2 + \varepsilon^2(a_1\sin\phi_1 - a\sin\phi)^2\,]^{3/2}}\mathrm{d}\phi\hat{\boldsymbol{j}}\,. \end{aligned} \tag{44}$$

As a check, we set $a_1 = 0$, and $\varepsilon = 1$. Thus we are calculating say E_x at the center of a circle. We find:

$$E_x = -\frac{\sigma}{a}\int_0^{2\pi}(\cos\phi)^2\,\mathrm{d}\phi = -\frac{\sigma\pi}{a}\hat{\boldsymbol{i}} \tag{45}$$

as expected [11]. However, in general it will be necessary to integrate equation (44), numerically.

The results of such calculations can be seen in figures 8(a), (b), for $\mathcal{D}^0_{xx}$ and $\mathcal{D}^0_{yy}$, where $x(y)$ are parallel to the (a, b)-axes, respectively.

On comparing the results for a square film, figures 4(a), (b), with those for an elliptical film, figures 8(a), (b), we see that there are similarities and differences. For example, both square and elliptical monolayers show a marked downturn in $\mathcal{D}^0_{xx}$, the *cliff edges*, as the uncompensated North and South poles are approached. However, for ellipses, the *cliff edge* extends into the sides of the film. This is also true for the $\mathcal{D}^0_{xy}$ term, where the spread in magnitude is even more apparent. In summary therefore, even a visual comparison between elliptical and rectangular films, with similar $(m_a,\ m_b)$ and $(m_x,\ m_y)$ values, suggests that the rectangular films will possess a greater number of spins experiencing the same local dipolar field.

8. The local field in a simple tetragonal system

Next, we examine the simplest tetragonal system, with unit-cell volume a^2b and ask the question: 'Is the local field equal to the Lorentz cavity field in a tetragonal system?'

If we align the z-axis along the b-axis, previous calculations for $\mathcal{D}^{\Delta k=0}_{xx}$ still hold $(z \equiv 0)$ (only x–y coordinates are involved). However, there will be differences in the values of $\mathcal{D}^{\Delta k=\pm1}_{xx}$ and $\mathcal{D}^{\Delta k=\pm2}_{xx}$. To probe this question we set $b = 1.1 \times a$, i.e. $\Delta z = 1.1a\Delta k$. We find:

$$\mathcal{D}^{\pm1.1}_{xx} = -0.085\ 2172;\ \ \mathcal{D}^{\pm2.2}_{xx} = -0.000\ 079\ 918. \tag{46}$$

Consequently, for a ferromagnet magnetized in-plane along say the x-axis:

$$\begin{aligned} \boldsymbol{B}_{\mathrm{DS}} &= \frac{\mu_0}{4\pi}\frac{1}{a^3}(D^0_{xx} + 2D^{\pm1.1}_{xx} + 2D^{\pm1.1}_{xx})\mu\hat{\boldsymbol{i}} = \frac{\mu_0}{4\pi}\frac{\mu}{a^2b}\frac{b}{a}4.34622\ \hat{\boldsymbol{i}} = \frac{\mu_0 M}{4\pi}4.78084\ \hat{\boldsymbol{i}} \\ &= \eta B_{\mathrm{Lor}}\ \hat{\boldsymbol{i}}\ (\eta = 1.14). \end{aligned} \tag{47}$$

So the local field is some 14% larger than the Lorentz field. This observation is not difficult to understand. The largest contribution to the local field B_{loc} is positive, coming from all the in-plane dipoles $(\Delta k = 0)$. All other planes contribute smaller negative contributions, which decrease very rapidly as Δk increases. Thus in the

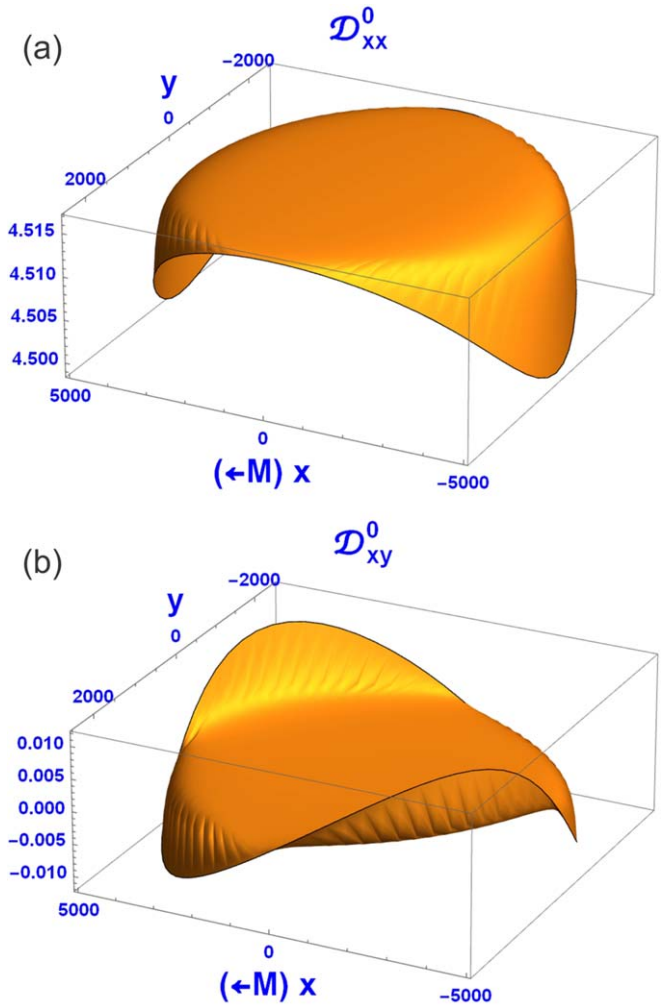

Figure 8. (a) The variation of $\mathcal{D}^0_{xx}$ as a function of position within a uniformly magnetized elliptical monolayer, magnetized along the positive x-axis. The ellipticity $\varepsilon = b/a = 0.5$. (b) The variation of $\mathcal{D}^0_{xy}$ as a function of position within a uniformly magnetized elliptical monolayer, magnetized along the positive x-axis. The ellipticity $\varepsilon = b/a = 0.5$.

case of a simple tetragonal system, with the longer b-axis perpendicular to the plane, an increase in local field is to be expected.

Such observations have consequences for FMR. For a thin infinite tetragonal film uniformly magnetized along the x-axis we may write:

$$\frac{\mathrm{d}\mu}{\mathrm{d}t} = -\gamma\mu \times \boldsymbol{B}_{\mathrm{eff}} = -\gamma\mu \times (\boldsymbol{B}_{\mathrm{app}} + \boldsymbol{B}_{\mathrm{ex}} + \boldsymbol{B}_{\mathrm{loc}})$$
$$= -\gamma \begin{pmatrix} \mu_x \\ \mu_y \\ \mu_z \end{pmatrix} \times \left(B_{\mathrm{app}} \begin{pmatrix} 1 \\ 0 \\ 0 \end{pmatrix} + \frac{\eta B_{\mathrm{Lor}}}{\mu} \begin{pmatrix} 1 & 0 & 0 \\ 0 & 1 & 0 \\ 0 & 0 & -2 \end{pmatrix} \begin{pmatrix} \mu_x \\ \mu_y \\ \mu_z \end{pmatrix} \right). \tag{48}$$

On making the usual small angle oscillation approximation namely: $\mu_y \mathrm{e}^{\mathrm{i}\omega t}$ and $\mu_z \mathrm{e}^{\mathrm{i}\omega t} \ll \mu_x (= \mu)$, we find:

$$\begin{pmatrix} 0 \\ \dot{\mu}_y \\ \dot{\mu}_z \end{pmatrix} = -\gamma \left(B_{\mathrm{app}} \begin{pmatrix} 0 \\ \mu_z \\ -\mu_y \end{pmatrix} + \eta B_{\mathrm{Lor}} \begin{pmatrix} 0 \\ 3\mu_z \\ 0 \end{pmatrix} \right). \tag{49}$$

Alternatively, as in a matrix equation:

$$\begin{pmatrix} \mathrm{i}\omega & \gamma(B_{\mathrm{app}} + \eta\mu_0 M) \\ -\gamma B_{\mathrm{app}} & \mathrm{i}\omega \end{pmatrix} \begin{pmatrix} \mu_y \\ \mu_z \end{pmatrix} = 0. \tag{50}$$

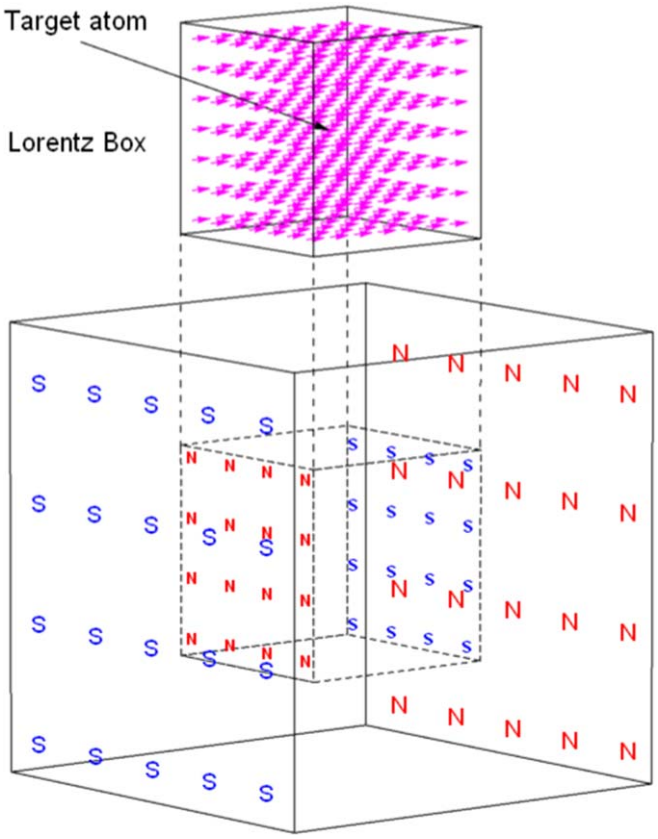

Figure 9. Schematic diagram showing the Lorentz box extracted from a ferromagnetic cube. The free poles on the inside of the Lorentz box give rise to the Lorentz remagnetizing field of $(+4\pi/3)M$ at the target atom, whilst the free poles on outside of the cube give rise to the de-magnetizing field of $(-4\pi/3)M$.

Equation (50) possesses the uniform-mode solution [6, 7]:

$$\omega = \gamma\sqrt{B_{\rm app}(B_{\rm app} + \eta\mu_0 M)}\,. \tag{51}$$

In practice, differences between this formula and the normal Kittel solution (with $\eta = 1$) may be difficult to spot. Furthermore, tetragonal systems will almost certainly exhibit anisotropy, which again will change the resonance condition [12]. Also, sometimes very thin layers appear to be characterized by demagnetization factors of other than -1 perpendicular to the film [12]. Nevertheless, the above discussion highlights the simple fact that only cubic systems are properly characterized by the Lorentz cavity field of $(\mu_0 M/3)$.

9. Lorentz demagnetization factor for a cube

In the bulk of this paper, we have been concerned primarily with the properties of thin films. However, it is of some interest to examine the situation in three dimensions. As we shall see, in section 10, this also has relevance to 2D monolayers with continuous magnetization.

First, imagine a ferromagnetic cube uniformly magnetized along say the x-axis. Second, imagine that a Lorentz box of magnetic moments is cut out and lifted out of the cube (metaphorically speaking), as illustrated schematically in figure 9 below. We set the dimensions of the Lorentz box equal to $(2i_0 + 1)^3$ where i_o is an integer.

We can now make the following familiar statements. One, the contribution of the dipole moments to the field at the center of the Lorentz box is zero: this is well known. So the field at the center of the Lorentz box is governed by the Lorentz remagnetizing field, arising from (i) the free poles on the *insides* of the empty box (which originally contained the Lorentz box of dipoles), and (ii) the demagnetization field, arising from the free poles on the *outside* edges of the overall cube. Once again, the surface charge analogy can be used to calculate the positive Lorentz remagnetizing field. We find:

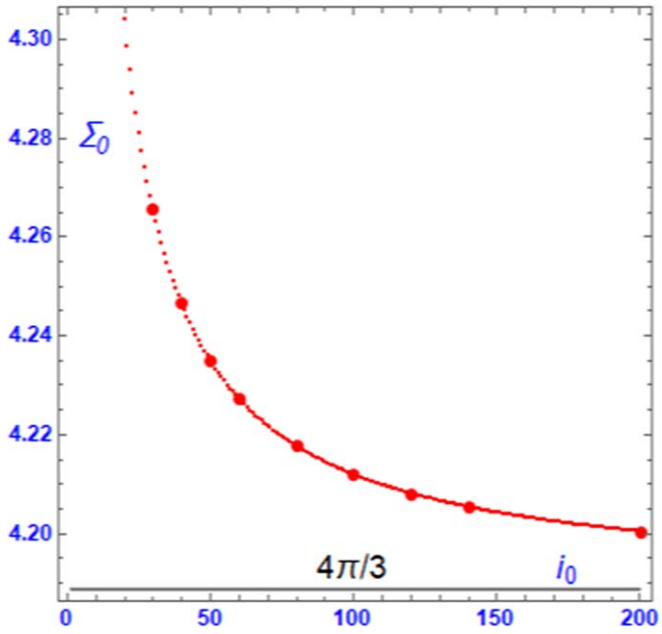

Figure 10. The double summation Σ_0 as a function of $x = i_0 a$.

$$E_x = \frac{2\sigma}{a^2}\sum_{j=-i_0}^{+i_0}\sum_{k=-i_0}^{i_0}\left(\frac{1}{i_0{}^2 + j^2 + k^2}\right)\cos\alpha$$
$$= \frac{2\sigma}{a^2}\sum_{j=-i_0}^{+i_0}\sum_{k=-i_0}^{i_0}\left(\frac{i_0}{(i_0{}^2 + j^2 + k^2)^{3/2}}\right) = \frac{\sigma}{a^2}\Sigma_0. \tag{52}$$

Here (i) the integers (i_0, j, k) are associated with the Cartesian vectors (x, y, z), and (ii) cos α is the direction cosine of the vector $\boldsymbol{E}$ with respect to the x-axis. The result of this calculation as a function of the size of the Lorentz cube, can be seen in figure 10. Once again, this data can be fitted with the asymptotic formula:

$$\Sigma_0 = 4.188\,83 - 2.303\,99/i_0. \tag{53}$$

Thus for large i_0, the double summation converges to $4\pi/3$, i.e.

$$E_x = \frac{2\sigma}{a^2}\Sigma_0 \rightarrow \frac{\sigma}{a^2}\frac{4\pi}{3}. \tag{54}$$

In summary therefore, for both spheres and *cubes*, the Lorentz remagnetizing factor of $4\pi/3$ is obtained. Nevertheless, even for i_0 as small as ~50, the error in the Lorentz remagnetizing field is only ~1.2%. So, in principle, similar methods to those advanced in sections 5 and 7, can be used to examine demagnetizing fields in uniformly magnetized 3D samples.

Next, we note that if the surface charge σ is spread uniformly over the sides of the cube, as in the continuum model, the double summation in equation (52) is readily converted into a double integral. We find:

$$E_x = \frac{2\sigma}{a^2}\Sigma_0 \rightarrow \frac{\sigma}{a^2}I_0, \tag{55}$$

where:

$$I_0 = 2\int_{-x_0}^{x_0} dy \int_{-x_0}^{x_0} dz \frac{x_0}{(x_0{}^2 + y^2 + z^2)^{3/2}} = 8\tan^{-1}\sqrt{\frac{1}{3}} = \frac{4\pi}{3}. \tag{56}$$

This result holds for any value of x_0, except zero. Also, if are dealing with a tetragonal system, it will be necessary to change the range of the integral in the z-direction. We find:

$$I_0 = 2\int_{-x_0}^{x_0} dy \int_{-x_0/n}^{x_0/n} dz \frac{x_0}{(x_0{}^2 + y^2 + z^2)^{3/2}} = 8\tan^{-1}\sqrt{\frac{1}{2n^2 + 1}}. \tag{57}$$

Once again therefore, the Lorentz cavity factor of $4\pi/3$ is obtained only in cubic systems.

As noted earlier, the field at the center of the Lorentz cube, of any size, is always zero. In terms of remagnetizing and demagnetizing fields, this result can be readily interpreted in terms of the remagnetizing field Lorentz $+\mu_0 M/3$, exactly canceling the demagnetizing field $-\mu_0 M/3$. However, this is not the case if the

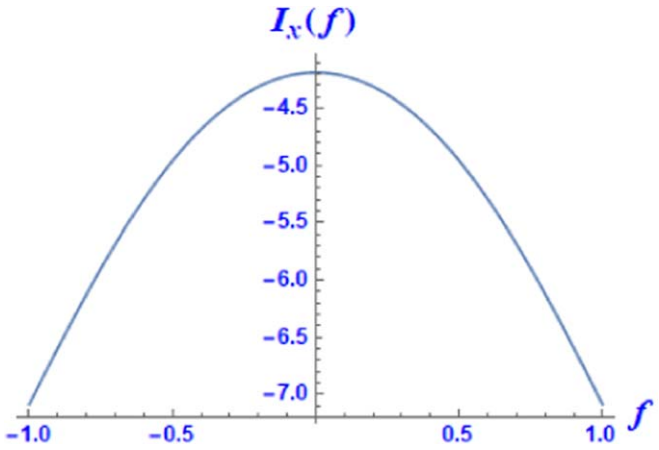

Figure 11. Variation of the demagnetizing field factor $I_x(f)$ along the x-direction, for $-1 \leqslant f \leqslant 1$.

Lorentz probe is moved away from the center of the ferromagnetic box. Here, the remagnetizing field, associated with the Lorentz probe stays the same, while the demagnetizing field associated with the distant surface *poles/charges* will change. Once again, the latter can be easily calculated using simple integrals, thereby allowing a fast determination of the variation of the local field across the bulk of say a ferromagnetic cube.

First, we examine the case of moving the Lorentz box across the ferromagnetic cube in the x-direction, with $y = z = 0$. Here we set the displacement along the x-axis as fx_0 where $-1 \leqslant f \leqslant 1$. We obtain:

$$\begin{aligned} I_x(f) = &-\int_{-x_0}^{x_0} \mathrm{d}y \int_{-x_0}^{x_0} \mathrm{d}z \frac{x_0(1-f)}{(x_0(1-f))^2 + y^2 + z^2)^{\frac{3}{2}}} \\ &- \int_{-x_0}^{x_0} \mathrm{d}y \int_{-x_0}^{x_0} \mathrm{d}z \frac{x_0(1+f)}{(x_0(1+f))^2 + y^2 + z^2)^{\frac{3}{2}}} \\ &= 4\{\cot^{-1}[(f-1)\sqrt{3+f(f-2)}] - \cot^{-1}[(f+1)\sqrt{3+f(f+2)}]\}. \end{aligned} \tag{58}$$

A plot of $I_x(f)$ can be seen in figure 11.

At zero displacement along the x-axis ($f = 0$), the Lorentz demagnetizing factor of $I_x(f = 0) = -4\pi/3$ is obtained. However, away from the center of the cube the strength of demagnetizing field rapidly increases, almost doubling as it reaches the faces of the Lorentz box. This result is in marked contrast to the monolayer results presented earlier in section 5. Clearly, the demagnetizing field associated with cube/rectangular boxes is highly non-uniform, in marked contrast to the situation encountered in uniformly magnetized spheres, discussed in the next section.

10. Local dipolar fields inside a uniformly magnetized sphere

Given the highly non-uniform demagnetization fields inside a ferromagnetic cube, it is of some interest to examine the case of a uniformly magnetized 3D sphere. Here it is well-known that the demagnetizing field is always $-\mu_0 M/3$, anywhere within the sphere. Thus if we use a smaller 3D sphere, as our Lorentz probe, it is easy to show that the local dipolar field is zero, at least up to the edge of the big sphere. Here, the Lorentz remagnetizing field from the small Lorentz spherical probe exactly cancels the demagnetizing field arising from the free poles on the edge of the big sphere. Of course, from a discrete point of view differences may be expected.

In figure 12, a discrete local field calculation can be seen for a sphere of radius 200 units. Note that the value of $\mathcal{D}^0_{xx}$ is shown right up to and beyond the edge of the sphere.

From an examination of figure 12, it is clear that well inside the sphere $\mathcal{D}^0_{xx}$ is close to zero, in accord with expectations. However as we approach the inside edge of the sphere, $\mathcal{D}^0_{xx}$ dips down before turning sharply upwards to a value of $\mathcal{D}^0_{xx} = 8.248$ right at the edge ($n = 200$). We conclude therefore that the local dipolar field is essentially equal to the applied field, except within a range of $\lesssim$10 units of the sphere radius. So despite classical expectations, the local dipolar field at or near the edge of the sphere is not equal to that at the center. Consequently, even for a sphere, some *pinning* of the FMR modes, at the edges, can be anticipated.

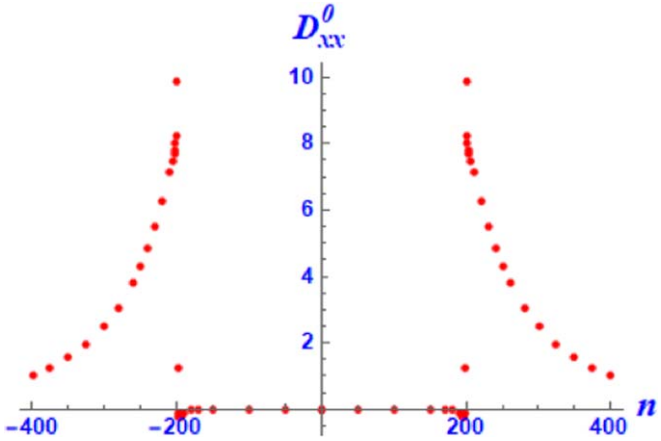

Figure 12. The value of $\mathcal{D}^0_{xx}$ for a traverse along the x-axis for a uniformly magnetized sphere, with a digital radius $n = 200$. Also shown for interest are the values outside the sphere.

Finally, we note that for x-axis trajectory taken in figure 12, the local dipolar field is given by:

$$\boldsymbol{B}_{\rm loc}(x,\,0,\,0) = \frac{\mu_0}{4\pi}\frac{1}{a^3}\begin{pmatrix} \mathcal{D}^{\Delta k}_{xx} & 0 & 0 \\ 0 & -\frac{1}{2}\mathcal{D}^{\Delta k}_{xx} & 0 \\ 0 & 0 & -\frac{1}{2}\mathcal{D}^{\Delta k}_{xx} \end{pmatrix}\begin{pmatrix} \mu_x \\ \mu_y \\ \mu_z \end{pmatrix}. \tag{59a}$$

Similarly, for the $y(z)$-trajectories:

$$\boldsymbol{B}_{\rm loc}(0,\,y,\,0) = \frac{\mu_0}{4\pi}\frac{1}{a^3}\begin{pmatrix} -\frac{1}{2}\mathcal{D}^{\Delta k}_{xx} & 0 & 0 \\ 0 & \mathcal{D}^{\Delta k}_{xx} & 0 \\ 0 & 0 & -\frac{1}{2}\mathcal{D}^{\Delta k}_{xx} \end{pmatrix}\begin{pmatrix} \mu_x \\ \mu_y \\ \mu_z \end{pmatrix} \tag{59b}$$

$$\boldsymbol{B}_{\rm loc}(0,\,0,\,z) = \frac{\mu_0}{4\pi}\frac{1}{a^3}\begin{pmatrix} -\frac{1}{2}\mathcal{D}^{\Delta k}_{xx} & 0 & 0 \\ 0 & -\frac{1}{2}\mathcal{D}^{\Delta k}_{xx} & 0 \\ 0 & 0 & \mathcal{D}^{\Delta k}_{xx} \end{pmatrix}\begin{pmatrix} \mu_x \\ \mu_y \\ \mu_z \end{pmatrix}. \tag{59c}$$

Consequently, for an x-axis direction of magnetization:

$$\boldsymbol{B}_{\rm loc}(0,\,y,\,0) = \boldsymbol{B}_{\rm loc}(0,\,0,\,z) = -\frac{1}{2}\boldsymbol{B}_{\rm loc}(x,\,0,\,0). \tag{60}$$

Similar identities can be established for other trajectories.

11. Continuous magnetization model

It is also of some interest to examine the case of 'continuous magnetization', widely used by the magnetic modeling community. Here we assume that every magnetic dipole is spread out uniformly over its unit-cell (a^3), thereby allowing discrete dipole summations to be replaced by simple integrals. For example, consider a single monolayer, containing the target atom at the origin, as illustrated schematically in figure 13.

In order to calculate the local field at the origin, we first empty the cubic cell (a^3) at the origin, and subsequently calculate the local field at the origin of the empty cell, generated by all the other dipoles in the monolayer. For an infinite film, we find:

$$\mathcal{D}^0_{xx} \to 4(I_1 + I_2 + I_3), \tag{61}$$

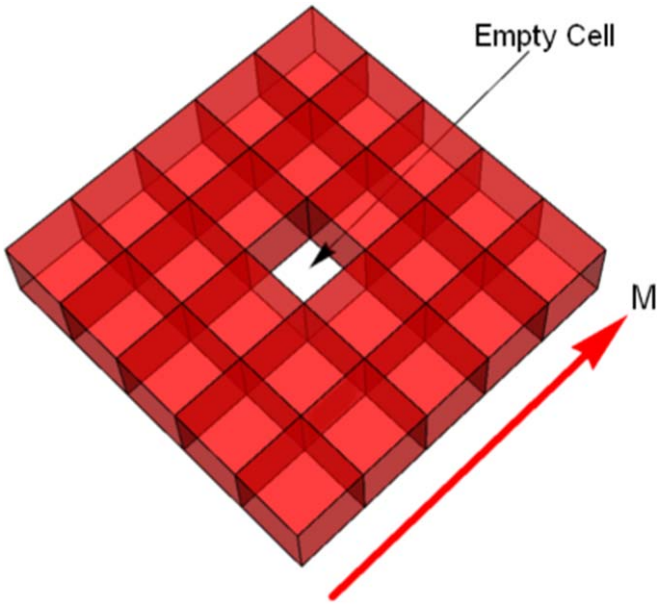

Figure 13. A section of a single monolayer with continuous magnetization, symbolized by red, with an empty cell at the origin.

where:

$$I_1 = \int_{\frac{1}{2}}^{\infty} \mathrm{d}x \int_{\frac{1}{2}}^{\infty} \mathrm{d}y \int_{-\frac{1}{2}}^{\frac{1}{2}} \mathrm{d}z \frac{(2x^2 - y^2 - z^2)}{(x^2 + y^2 + z^2)^{\frac{5}{2}}} = \frac{\pi}{6}$$

$$I_2 = \int_{0}^{1/2} \mathrm{d}x \int_{\frac{1}{2}}^{\infty} \mathrm{d}y \int_{-\frac{1}{2}}^{\frac{1}{2}} \mathrm{d}z \frac{(2x^2 - y^2 - z^2)}{(x^2 + y^2 + z^2)^{\frac{5}{2}}} = -\frac{\pi}{6}$$

$$I_3 = \int_{1/2}^{\infty} \mathrm{d}x \int_{0}^{1/2} \mathrm{d}y \int_{-1/2}^{1/2} \mathrm{d}z \frac{(2x^2 - y^2 - z^2)}{(x^2 + y^2 + z^2)^{5/2}} = \frac{\pi}{3}. \tag{62}$$

Thus in the continuum model, the Lorentz cavity field factor at the origin is given by:

$$\mathcal{D}^0_{xx} = 4(I_1 + I_2 + I_3) = 4\pi/3. \tag{63}$$

Of course, one must also consider other possible contributions from neighboring monolayers. For the nearest neighbor upper monolayer layer the contribution to the target site takes the form:

$$\mathcal{D}^1_{xx} \rightarrow 4(I_1 + I_2 + I_3 + I_4). \tag{64}$$

Note that this time, the integral contains the contribution arising from $i = j = 0$ term. We find:

$$I_1 = \int_{\frac{1}{2}}^{\infty} \mathrm{d}x \int_{\frac{1}{2}}^{\infty} \mathrm{d}y \int_{-\frac{1}{2}}^{\frac{1}{2}} \mathrm{d}z \frac{(2x^2 - y^2 - (z+1)^2)}{(x^2 + y^2 + (z+1)^2)^{\frac{5}{2}}} = 0.251\,32$$

$$I_2 = \int_{0}^{1/2} \mathrm{d}x \int_{\frac{1}{2}}^{\infty} \mathrm{d}y \int_{-\frac{1}{2}}^{\frac{1}{2}} \mathrm{d}z \frac{(2x^2 - y^2 - (z+1)^2)}{(x^2 + y^2 + (z+1)^2)^{\frac{5}{2}}} = -0.251\,32$$

$$I_3 = \int_{\frac{1}{2}}^{\infty} \mathrm{d}x \int_{0}^{\frac{1}{2}} \mathrm{d}y \int_{-\frac{1}{2}}^{\frac{1}{2}} \mathrm{d}z \frac{(2x^2 - y^2 - (z+1)^2)}{(x^2 + y^2 + (z+1)^2)^{\frac{5}{2}}} = 0.211\,716$$

$$I_4 = \int_{0}^{1/2} \mathrm{d}x \int_{0}^{1/2} \mathrm{d}y \int_{-\frac{1}{2}}^{\frac{1}{2}} \mathrm{d}z \frac{(2x^2 - y^2 - (z+1)^2)}{(x^2 + y^2 + (z+1)^2)^{\frac{5}{2}}} = -0.211\,716. \tag{65}$$

Thus $\mathcal{D}^1_{xx} = 0$. This is also true for the second nearest layer $\mathcal{D}^2_{xx}$ etc. In conclusion therefore the continuous model predicts that only that monolayer containing the origin contributes to the local dipolar field, and that that contribution is determined by $\mathcal{D}^0_{xx} = 4\pi/3$. This of course, is exactly equal to the Lorentz remagnetizing field factor, but this time arising from the walls of a single unit cubic cell. In summary, the above constitutes a *proof* of the Lorentz method (see appendix) as applied to a thin magnetic monolayer. Here the magnetization is continuous, divergence free, and the only free surface poles are those on the inside of the single-cell Lorentz box.

Finally, we note that the predicted FMR frequency of a single monolayer is equal to that of the discrete model, provided we make the following assumptions. One, we empty out the unit cell, as shown in figure 13. Two, place a single magnetic point-dipole at the center of the empty cell. Three, calculate the local field at the single point-dipole arising from all other dipoles in the monolayer, now assumed to be continuous.

12. Conclusions and discussions

In this paper, an extension of the Lorentz method has been discussed which is subsequently used to study the variation of local dipolar fields across thin films/monolayers, and in some 3D systems. In particular, we have concentrated on determining demagnetizing fields arising from uncompensated magnetic poles at the edges of rectangular and elliptical films, using the electrostatic analogy. Initially, it was hoped that a particular shape of thin film could be identified which offered a constant demagnetization field, inside the sample. In essence, a 2D equivalent of 3D spheres and ellipses, which both offer a constant demagnetization field inside the sample, regardless of position. Sadly, no such 2D shape has been found. However, long thin rectangular shapes, magnetized along the long axis, offer the best compromise, and should therefore be the choice of sample for FMR applications, and possible incorporation into hybrid magnetic metamolecules.

Finally, some readers may question the usefulness or otherwise of planar monolayer studies. We answer as follows. Firstly, it has been shown that a minimum of five monolayers is required to generate the expected Lorentz cavity field in thin films (see section 3 of this paper, and [11]). Secondly, recently, 2D-magnetism has been observed in a single monolayer of CrI_3 [13, 14]. Here, magnetocrystalline anisotropy at the Cr sites negates the famous Mermin–Wagner theorem, which states that no magnetic order can exist in isotropic 1D or 2D systems [15]. Thirdly, the properties of hyper-thin film dielectrics are of commercial importance [16]. Here, the Lorentz field factor plays a crucial role in the determination of the local electric field, and hence possible electrical breakdown. More dielectric applications of the Lorentz method, and the subsequent extension to the Clausius–Mossiti relationship, can be found in [17, 18].

Acknowledgments

The authors acknowledge the Engineering and Physical Sciences Research Council (EPSRC) under Grant Numbers EP/P021190/1, EP/P020151/1, and EP/P02047X/1.

Appendix A. The Lorentz method of surface charges

Following Kittel and Lorentz, we use the electrostatic analogy. For convenience, the proof given here is that of Kittel [8], p 450, but in SI units and with minor corrections.

The electrostatic potential from a dipole with a dipole moment $\boldsymbol{p}$ ($p = qa$) takes the form

$$V(\boldsymbol{r}) = \frac{1}{4\pi\epsilon_0}\left(\frac{\boldsymbol{p}.\boldsymbol{r}}{r^3}\right) = -\frac{1}{4\pi\epsilon_0}\boldsymbol{p}.\mathrm{grad}\left(\frac{1}{r}\right). \tag{A.1}$$

Next, we adopt the macro-field approach where the dipole moment $\boldsymbol{p}$ is spread uniformly over the unit cell, giving rise to a macroscopic polarization $\boldsymbol{P}$. Thus, in the continuum model:

$$V(\boldsymbol{r}) = -\frac{1}{4\pi\epsilon_0}\int \boldsymbol{P}.\mathrm{grad}\left(\frac{1}{r}\right)\mathrm{d}V. \tag{A.2}$$

Here, it is understood that (i) the point $\boldsymbol{r}$ is far away from the volume of polarization in question, so that when viewed from $\boldsymbol{r}$ the polarization looks uniform, and (ii) the integral is taken over the volume of polarized material.

Next, we use a vector identity to write:

$$V(\boldsymbol{r}) = -\frac{1}{4\pi\epsilon_0}\int\left(-\frac{1}{r}\mathrm{div}\boldsymbol{P} + \mathrm{div}\frac{\boldsymbol{P}}{r}\right)\mathrm{d}V. \tag{A.3}$$

However, if the polarization $\boldsymbol{P}$ is uniform, $\mathrm{div}\boldsymbol{P} = 0$ and so:

$$V(\boldsymbol{r}) = -\frac{1}{4\pi\epsilon_0}\int \mathrm{div}\frac{\boldsymbol{P}}{r}\mathrm{d}V. \tag{A.4}$$

Finally, on invoking the Gauss theorem, the volume integral in equation (4) is transformed into a surface integral:

$$V(\boldsymbol{r}) = -\frac{1}{4\pi\epsilon_0}\int\frac{P_N}{r}\mathrm{d}S = -\frac{1}{4\pi\epsilon_0}\int\frac{q_N}{r}\mathrm{d}S\,. \tag{A.5}$$

Here q_N is an effective charge normal to the surface of the polarized object. Thus the determination of the potential $V(\boldsymbol{r})$, arising from a host of electric dipoles has been reduced to a calculation of the potential arising from a surface charge distribution q_N.

Finally, rather than the potential $V(\boldsymbol{r})$, we need the electric field $\boldsymbol{E}(\boldsymbol{r})$:

$$\boldsymbol{E}(\boldsymbol{r}) = -\mathrm{grad}(V(\boldsymbol{r})) = +\frac{1}{4\pi\epsilon_0}\mathrm{grad}\left(\int\frac{q_N}{r}\mathrm{d}S\right). \tag{A.6}$$

The key feature in the Lorentz procedure is that from the viewpoint of $\boldsymbol{r}$, the polarized object must look like a continuum with uniform polarization $\boldsymbol{P}$.

Appendix B. Spin-wave $k = \pi/l$ mode in a permalloy film

Here we use Weber's spin-wave resonance results on permalloy [19] (see also Kittel [8], p 600) to obtain estimates for (i) homogeneous broadening of the FMR linewidth, and (ii) the spin-wave stiffness constant D.

First, we assert that 'damping', as inscribed in the Landau–Lifshitz–Gilbert equation of motion, leads to 'homogeneous broadening' of the FMR resonance. We maintain that this sets an ultimate limit on the FMR linewidth. From Weber's results on a 500 nm thick permalloy film, we find:

$$\Delta B_{\mathrm{Homo}} \approx 9 \times 10^{-3}\ (\mathrm{T}). \tag{B.1}$$

Secondly, from Weber's observation of the well separated $n = 7$–17 (n odd) spin-wave modes, in the thickness t of the permalloy film, it is possible to obtain a value for the spin-wave stiffness constant D. Explicitly:

$$\omega = \gamma(B_{\mathrm{app}} - \mu_0 M) + Dk^2 = \gamma(B_{\mathrm{app}} - \mu_0 M + \Delta B_D n^2) \quad \Delta B_D = \frac{D}{\gamma}\left(\frac{\pi}{t}\right)^2. \tag{B.2}$$

We find:

$$\Delta B_D = 8.2445 \times 10^{-4}(\mathrm{T});\ \mu_0 M = 1.053\ (\mathrm{T}). \tag{B.3}$$

Thirdly, if the spins in the 'so-called' uniform mode $k = 0$ are pinned at the North/South pole *cliff-edges*, there will be an additional energy shift associated with the presence of the $k = \pi/l$ spin-wave, in the plane of the rectangular strip. This situation is illustrated schematically, in figure B1. However if the field shift due to the spin wave is say ten times less than the homogeneous linewidth ΔB_{Homo}, Kittel's $k = 0$ FMR formula will still be acceptable. After some minor manipulation, we find that the length of such a film should be $l \geqslant 500$ nm, in the direction of magnetization.

Finally, we make two more remarks. One, in the above discussion, it has been assumed that the 'pinning' is uniform at the North and South pole cliff edges. However, the situation in the corners of the film may lead to extra complexity (see figure 4(b) and [20] for more exotic FMR modes, on smaller platelets, pumped and probed by optical techniques). Two, the Lorentz method must fail, in principle, in the presence of a spin-wave. Here the divergence of the magnetization div($\boldsymbol{M}$) is no longer zero (see appendix A). For small amplitudes of oscillation,

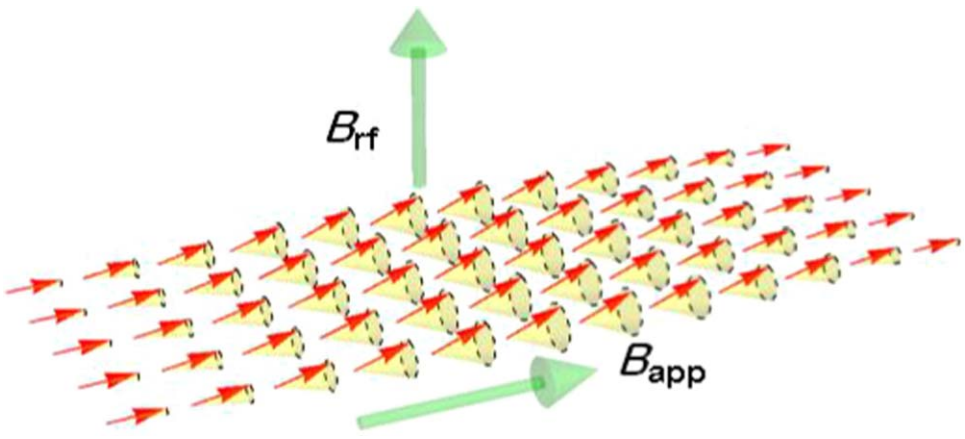

Figure B1. A monolayer of spins precessing in the presence of an applied field. All the spins are precessing in-phase. However, the amplitude of their individual precessions is now x-dependent, given that the spins are pinned at the North and South pole *cliff-edges*. The wavelength of the spin-wave is $2l$ where l is the length of film in the x-direction of magnetization.

this failure in principle is probably of little relevance. However for larger turn angles, of say of up to 90°, it would constitute a serious issue.

ORCID iDs

G van der Laan https://orcid.org/0000-0001-6852-2495
T Hesjedal https://orcid.org/0000-0001-7947-3692

References

[1] Stenning G B G, Bowden G J, Lewis L C, Maple C, Gregory S A, Sposito A, Eason R W, Zheludev N I and de Groot P A J 2013 Magnetic control of a meta-molecule *Opt. Express* **21** 1456
[2] Gregory S A, Stenning G B G, Bowden G J, Zheludev N I and de Groot P A J 2014 Giant magnetic modulation of a planar, hybrid metamolecule resonance *New J. Phys.* **16** 063002
[3] Gregory S A, Maple L C, Stenning G B G, Hesjedal T, van der Laan G and Bowden G J 2015 Angular control of a hybrid magnetic metalmolecule using anisotropic FeCo *Phys. Rev. Appl.* **4** 054015
[4] Bhoi B, Kim B, Kim J, Cho Y-J and Kim S-K 2017 Robust magnon-photon coupling in a planar geometry hybrid of inverted split ring resonator and YIG film *Sci. Rep.* **7** 11930
[5] Kruglyak V V, Demokritov S O and Grundler D 2010 Magtronics *J. Phys. D: Appl. Phys.* **43** 264001
[6] Woo S, Delaney T and Beech G S D 2017 Magnetic domain wall pinning assisted by spin-wave bursts *Nat. Phys.* **13** 448
[7] Kittel C 1948 On the theory of ferromagnetic resonance absorption *Phys. Rev.* **73** 155
[8] Kittel C 1971 *Introduction to Solid State Physics* 4th edn (New York: Wiley)
[9] Lorentz H A 1916 *The Theory of Electrons and its Application to the Phenomena of Light and Radiant Heat* (Leipzig: Teubner)
[10] Brown W F 1962 *Magnetostatic Principles in Ferromagnetism* (Amsterdam: North-Holland)
[11] Bowden G J, Stenning G B G and van der Laan G 2016 Asymptotic behavior of local dipolar fields in thin films *J. Magn. Magn. Mater.* **416** 449
[12] Farle M 1998 Ferromagnetic resonance of ultrathin metallic layers *Rep. Prog. Phys.* **61** 755
[13] Huang B *et al* 2017 Layer dependent ferromagnetism in a van der Waals crystal down to the monolayer limit *Nature* **546** 270
[14] Frisk A, Duffy L B, Zhang S, van der Laan G and Hesjedal T 2018 Magnetic x-ray spectroscopy of two-dimensional CrI_3 layers *Mater. Lett.* **231** 5
[15] Mermin N D and Wagner H 1966 Absence of ferromagnetism or antiferromagnetism in one or two dimensional isotropic Heisenberg models *Phys. Rev. Lett.* **17** 1133
[16] McPherson J W 2015 Lorentz factor determination for local electric fields in semiconductor devices using hyper-thin dielectrics *J. Appl. Phys.* **118** 204106
[17] Vanzo D, Topham B J and Soos Z G 2015 Dipole-field sums, Lorentz factors, and dielectric properties of organic molecular films modeled as crystalline arrays of polarizable points *Adv. Funct. Mater.* **25** 2004
[18] D'Avino G, Vanzo D and Soos Z G 2016 Dielectric properties of crystalline organic molecular films in the limit of zero overlap *J. Chem. Phys.* **144** 034702
[19] Weber R 1968 Spin-wave resonance *IEEE Trans. Magn.* **4** 28
[20] Kruglyak V V, Barman A, Hicken R J, Childress J R and Katine J A 2005 Picosecond magnetization dynamics in nanomagnets: crossover to nonuniform precession *Phys. Rev.* B **71** 220409(R)